

# Comprehensive Evaluation of Prototype Neural Networks

Philipp Schlinge<sup>1\*</sup>, Steffen Meinert<sup>1</sup> and Martin Atzmueller<sup>1,2</sup>

<sup>1</sup>Semantic Information Systems Group,  
Osnabrück University, Wachsbleiche 27, 49090, Osnabrück, Germany.

<sup>2</sup>Research Department Cooperative and Autonomous Systems,  
German Research Center for Artificial Intelligence (DFKI),  
Hamburger Str. 24, 49084, Osnabrück, Germany.

\*Corresponding author(s). E-mail(s): [philipp.schlinge@uos.de](mailto:philipp.schlinge@uos.de);  
Contributing authors: [steffen.meinert@uos.de](mailto:steffen.meinert@uos.de); [martin.atzmueller@uos.de](mailto:martin.atzmueller@uos.de);

## Abstract

Prototype models are an important method for explainable artificial intelligence (XAI) and interpretable machine learning. In this paper, we perform an in-depth analysis of a set of prominent prototype models including *ProtoPNet*, *ProtoPool* and *PIPNet*. For their assessment, we apply a comprehensive set of metrics. In addition to applying standard metrics from literature, we propose several new metrics to further complement the analysis of model interpretability. In our experimentation, we apply the set of prototype models on a diverse set of datasets including fine-grained classification, Non-IID settings and multi-label classification to further contrast the performance. Furthermore, we also provide our code as an open-source library, which facilitates simple application of the metrics itself, as well as extensibility – providing the option for easily adding new metrics and models. <https://github.com/uos-sis/quanproto>

**Keywords:** Interpretable AI, Prototype-based Models, Explainable AI

## 1 Introduction

While there have been enormous advances in deep learning [1, 2], the challenge of developing truly interpretable models with accuracy comparable to their black-box counterparts remains unresolved [3, 4, 5]. This is a prominent and active area of research connecting both interpretability and explainability of the respective models [6]. In particular, in the domain of image-related tasks like classification, non-interpretable models typically outperform most other models or techniques. However, in high-risk domains often encountered in industry or the medical sectors, explainability

and interpretability are key requirements [7, 8], also enabling computational sensemaking [9].

Different post-hoc techniques have been developed in the past, such as SHAP and LIME [10, 11]. These explain the decision of a model by calculating the importance of individual input features and can be applied to a large family of models. In the domain of image classification, saliency maps are a particular prominent subgroup of these model-agnostic methods, e.g., Integrated Gradients, Grad-CAM and other variants explain the attribution of individual or groups of pixels for a given prediction [12, 13]. Although, such model-agnostic techniques are widely used and

can provide considerable insight into trained models, they are in themselves only post-hoc methods with several drawbacks, e.g., [14] compared to a completely intrinsically interpretable model.

One possible solution to overcome some of these problems, has been the development of deep part-based prototype models, firstly presented in [15] and [16]. A key advantage is their intrinsic interpretability. Part-based prototype models focus on learning a meaningful embedding space using an often pre-trained black-box network as feature extractor. A key distinction from standard black-box models is the aim to extract features that concentrate on specific sections of the image. This division of the image in the embedding space allows the network to learn prototypes that represent only particular parts of the object. The classification layer then utilizes the presence of a prototype in the image to calculate the prediction. To provide an explanation for a prediction, the prototypes that have the highest evidence are projected back to the input space through a saliency method. This simple visual representation of important image parts typically allows even non-technical users to understand the model’s decision process.

Our research is based on and extends the work of Nauta et al. [17]. With an implementation of a substantial portion of the evaluation framework presented in [17], we facilitate a thorough assessment of part-based prototype models. Our contributions are summarized as follows:

1. We expand the set of metrics referenced in [17] by proposing several novel metrics designed to enhance the interpretability assessment of part-based prototype models.
2. Specifically, we provide an implementation of 22 metrics, including 13 novel contributions, via our open-source library *QuanProto*.
3. Furthermore, we conducted a comprehensive analysis of three prominent part-based prototype models, i.e., *ProtoPNet* [16], *ProtoPool* [18] and *PIPNet* [19]. We provide new insights and demonstrate the utility and applicability of our library.
4. Our evaluation offers a broad perspective on potential application scenarios by utilizing established datasets such as *CUB200* [20] and *Cars196* [21] while also extending to a more practice-oriented Non-IID context with the

*NICO* [22] dataset and a multi-label classification task focused on the challenge of learning class-independent features from animals using the *AWA2* [23] dataset.

## 2 Related Work

Below, we start with a brief summary of concept-based artificial intelligence, before describe architectures, limitations, and evaluation methods of deep learning-based part-prototype models. For a comprehensive survey on classical prototype models, we refer to Biehl et al. [24].

### *Concept-based Artificial Intelligence*

Central to concept-based explanation is the notion of conceptualization [25] and concepts which has already been investigated in different fields, most notably in case-based reasoning [26, 27]. The basic idea is to focus on human understandable higher-order concepts not only related to single features. Here, a recent and closely related direction is concept-based artificial intelligence [28]. Examples of this approach are e.g., concept bottleneck models [29] or concept activation vectors [30]. Another approach, which shares similarities with prototype-based models, is *TesNet* by Wang et al. [31]. Here, an interpretable embedding space constructed by basis-concepts is learned.

### *Architectures*

The prototypical part network (*ProtoPNet*) from Chen et al. [16] is one of the pioneering networks that popularized the concept of part prototype networks in image classification. In addition to the models examined in this article, other networks have been developed that combine the prototype approach with many concepts from the ML field. Nauta et al. [32] varied the classification process, by replacing the fully connected layer at the end of the model through a decision tree (*ProtoTree*) [32]. *ProtoPShare* [33] uses an iterative post-processing technique to merge prototypes from a *ProtoPNet* model, effectively creating shared prototypes between classes and reducing the amount of needed prototypes. Xue et al. [34] adapted the idea of *ProtoPNet* to be used together with vision transformers as feature extractors. Prototype-based deep learning models have also been used for time series [35],

graph data [36], or image segmentation tasks [37]. There is also work, which combines deep prototype models with an autoencoder architecture [38]. Other variants of the *ProtoPNet* architecture, include [39], [40], [41], [42].

### ***Application Domain***

Part-based prototype models have been used e. g., to inspect power grids visually [43], in the classification of MRI scans to detect Alzheimer’s disease [44] or X-Ray images to classify Chest X-rays [45]. Carlone et al. [46] propose a prototype-based model to identify breast cancer, highlighting the acceptance of visual explanations.

### ***Limitations***

Besides the success of *ProtoPNet* and the improvement through architectural changes, there are also limitations and some critique regarding the way the prototypical networks explain their decisions. Xu-Darme et al. [47] criticize the way *ProtoPNet* and *ProtoTree* visualize the learned prototypes and propose to use different saliency methods to overcome this problem. Hoffmann et al. [48] point out that *ProtoPNets* struggle with adversarial examples or compression artifacts in the input. Nevertheless, Hoffmann et al. do not want to dispute part prototypical networks, but raise the awareness of these problems.

### ***Evaluation of Prototypical-Part Models***

In the literature, there have been several approaches aiming at evaluating different prototypical-part models. These include different evaluation methods as well as specific metrics. The work of Huang et al. [49], e. g., proposes two metrics called *consistency score* and *stability score* that focus on the semantic properties of prototypes alongside a new network architecture to improve these metrics. Recently, there has also been work to create frameworks to simplify the utilization of different types of part-based prototype models, cf. *ProtoPNeXt* [50] and the work on the library *CaBRNet* [51]. Ma et al. [52], try to improve the visualization of the prototypes using multiple examples from the training set to describe the concept behind a learned prototype. The framework *HIVE*, created by Kim et al. [45], is designed for the evaluation of explanation techniques. They highlight key issues that are crucial

when humans must interpret these explanations. Nauta et al. [53] examine, why the model considers a prototype and a patch of the input image as similar. A comprehensive survey focusing on the interpretability assessment of part-based prototype models is also given by Nauta et al. [17].

## **3 Datasets**

For evaluating the respective networks in diverse domains, we selected several datasets from the areas of (multi-label) classification, in particular fine-grained prototypical classification, and general object detection in a Non-IID setting.

### ***Caltech-UCSD Birds (CB200) Dataset***

The first fine-grained dataset is Caltech-UCSD Birds-200-2011 (*CUB200*) [20], that features a challenging collection of bird species. This dataset is frequently used as a benchmark for part-based prototype methods. The rich annotations allow for a detailed evaluation of the importance of individual object parts in the classification process, enabling a comprehensive assessment of the prototypes. The dataset contains 11,788 images of 200 bird species with segmentation masks, bounding boxes, part locations, and attribute labels.

### ***Stanford Cars Dataset (Cars 196)***

For our second fine-grained dataset, we selected the Stanford Cars dataset (*Cars196*), introduced by Krause et al. [21]. Unlike the natural objects in the *CUB200* dataset, this dataset focuses on fine-grained classification of manufactured objects, and is similarly used to benchmark part-based prototype methods. It consists of 16,185 images of 196 car models, covering a wide range of vehicle types including sedans, SUVs, coupes, convertibles, pickups, and hatchbacks.

### ***NICO Dataset***

For general object detection in a Non-IID setting, we used the *NICO* Dataset from He et al. [22]. This dataset includes 10 animal classes and 9 vehicle classes, though our focus is on the animal classes. Each class is further divided into 10 context categories representing various environments, attributes, and activities. The dataset contains 12,980 images of animals. Essentially, this Non-IID setting is a more realistic scenario,

which is also new for part-based prototypical models. Hence, we want to apply this setting mainly through different background environments in the training and test sets to assess if the networks naturally promote object-focused prototypes. Since this cannot be achieved using the provided context categories (as few represent distinct environments), we use a simple image analysis inspired by Cheng et al. [54], based on the HSV color space [55], to split the dataset into training/validation and test sets. This approach effectively creates a Non-IID scenario with varying distributions across training and test data. Further details are given in the implementation.

### *Animals with Attributes (AWA2) Dataset*

The last dataset is Animals with Attributes 2 (AWA2) introduced by Xian et al. [23]. This dataset is a benchmark for attribute-based classification, a related model domain to part-based prototype models. The dataset comprises 37,322 images across 50 animal classes, with binary and continuous class attributes. For evaluating the performance of part-based prototype methods in a multi-label classification setting, we focus on the given attributes. The AWA2 dataset includes 85 attributes that are used to describe a class. Since not all attributes describe visible features, we only use a subset of all attributes, i. e., those corresponding to the 49 visible attributes.

## 4 Prototype Networks

Because this work focuses on a comprehensive set of metrics. We kept our set of models small and selected three prominent networks based on the following criteria: class-specific vs. shared prototypes and explicit vs. indirect prototype representations. We chose *ProtoPNet* [16], the first popular prototype model, that uses class-specific explicit prototype vectors. We further include the *ProtoPool* [18] model as a representative for shared and explicit prototype learning. Finally, we chose *PIPNet* [19] as a recently introduced architecture for the shared and indirect case.

Each network uses a similar architecture visualized in Figure 1, the components are labelled with the letters (A)-(F) in the figure: Starting with a deep neural network (A) as backbone. This network extracts a feature map (B) from the input

image. The important characteristic of a part-based prototype model is to calculate the presence of prototypes in the feature map. In the case of a model with specific prototypes, each prototype (C) is compared with the feature vectors in (B) resulting in a set of similarity maps (D). In the case of indirect prototypes, the feature map is further processed and directly interpreted as a collection of similarity maps (D) without an explicit comparison. The final classification (F) is then obtained based on the highest similarity score (E) in each map.

Below, we summarize each applied prototype network architecture, highlighting the unique design choices and training procedures.

### *ProtoPNet*

The first network is *ProtoPNet*. It follows the general architecture shown in Figure 1 consisting of a convolutional neural network as a backbone followed by two additional  $1 \times 1$  convolutional layers to adjust the output dimension  $D$ . This results in a feature map  $\mathbf{z} \in \mathcal{R}^{H \times W \times D}$  with individual vectors  $\tilde{\mathbf{z}} \in \mathcal{R}^{1 \times 1 \times D}$ . The feature map is then processed by a prototype layer, that holds a set of  $n$  prototypes  $\mathbf{P} = \{\mathbf{p}_m\}_{m=1}^n$  with  $\mathbf{p}_m \in \mathcal{R}^{1 \times 1 \times D}$ , such that each prototype has the same dimensions as one feature vector. A pre-determined number of prototypes  $m_k$  is allocated for each class  $k \in \{1, \dots, K\}$ . The prototype layer computes a set of similarity maps  $\mathbf{A} = \{\mathbf{a}_m\}_{m=1}^n$  based on the squared L2 distance between a prototype and a feature vector as follows:

$$\mathbf{a}_m = \left\{ \log \left( \frac{\|\tilde{\mathbf{z}} - \mathbf{p}_m\|_2^2 + 1}{\|\tilde{\mathbf{z}} - \mathbf{p}_m\|_2^2 + \epsilon} \right) \mid \tilde{\mathbf{z}} \in \mathbf{z} \right\} \in \mathcal{R}^{H \times W \times 1} \quad (1)$$

The similarity score of a prototype is then calculated using a max pooling operation  $\mathbf{s}_m = \max(\mathbf{a}_m)$  and lastly used in the fully connected layer to make the classification.

*ProtoPNet* uses a multistep training process, separating the training of the last layer from the rest of the network. At the beginning, the last layer is initialized using 1 for weights connecting a prototype to its corresponding class and  $-0.5$  otherwise. This ensures the learning of class specific prototypes. The first training step optimizes the backbone and prototype layer to learn a meaningful latent space, clustering prototypes

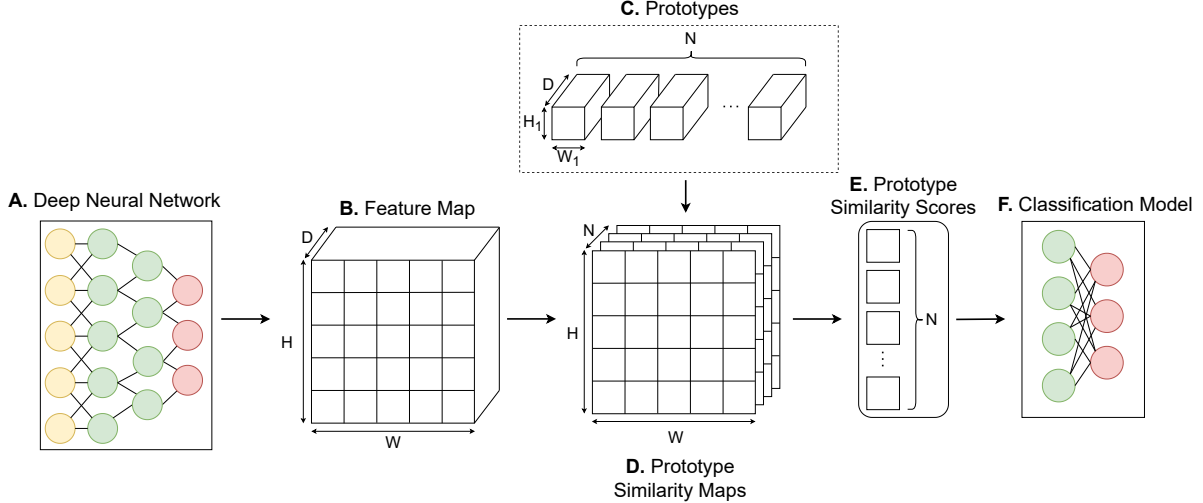


**Fig. 1** A visual representation of a prototype-based neural network. Starting from (A) a deep neural network, such as ResNet, extracting a feature map (B), the model identifies the presence of prototypes (C) by comparing them with feature vectors; generating similarity maps (D). Classification (F) is performed according to the highest similarity scores (E) derived from these maps

from the same class and separating them from prototypes of other classes. This is done using a linear combination of a classification loss and two novel losses, the cluster loss and separation loss  $\lambda_C \mathcal{L}_C + \lambda_{cl} \mathcal{L}_{cl} + \lambda_{sep} \mathcal{L}_{sep}$ . In the second step, each prototype is first projected onto the nearest feature vector from its assigned class. The last layer is then fine-tuned to improve classification performance, using only the classification loss and an L1 regularization term to keep the positive reasoning characteristic. Chen et al. [16] observed that some prototypes focus on the background. These prototypes contradict the goal of the model to learn class-specific object parts. To address this, the authors propose a pruning step after training, which removes such prototypes. We use both the original and pruned version in the evaluation to analyze the effectiveness of this approach.

### ProtoPool

The *ProtoPool* [18] model by Rymarczyk et al., addresses several limitations of *ProtoPNet*. It introduces a new similarity function and an automatic, fully differentiable assignment of prototypes to classes, that enables the network to learn shared prototypes. The model itself follows the architecture of *ProtoPNet* consisting of a CNN backbone with additional convolutional layer to adjust the output shape, a prototype layer, and

a fully connected layer. The prototype layer contains a set of  $n$  trainable prototypes  $\mathbf{P} = \{\mathbf{p}\}^n$  with  $\mathbf{p} \in \mathcal{R}^{1 \times 1 \times D}$ , similar to *ProtoPNet*. A novel part is the assignment matrix with  $L$  prototype slots for each class, where each slot is implemented as a distribution  $q_l \in \mathbb{R}^N$  over all available prototypes. The similarity maps  $\mathbf{A} = \{\mathbf{a}\}^n$  are computed using the same equation 1 as in *ProtoPNet*. To enhance prototype locality, the authors introduce a focal similarity function, which computes the difference between the maximum similarity and the average similarity as follows:

$$g = \max(\mathbf{a}) - \text{mean}(\mathbf{a}) \quad (2)$$

After calculating all similarity scores, the assignment matrix is used to compute an aggregated similarity value  $g_l$  for each slot of a class as follows  $g_l = \sum_{i=1}^N q_l^i g_i$ , which is then used in the fully connected layer to make the final prediction.

*ProtoPool* follows the same multistep training process as *ProtoPNet*. In the first step, the last layer is initialized with a 1 for a slot assigned to a class and 0 otherwise, and then fixed during the training of the backbone and prototype layer. The optimization uses classification loss, cluster loss, and separation loss as in *ProtoPNet*. To learn the distributions  $q_l$ , the authors

apply a Gumbel-Softmax layer, that adds additional noise to the distribution at the start of the training process. This noise is then reduced during the training period, so the distribution can converge to a one-hot encoded vector. To prevent that a prototype is assigned to multiple slots of the same class, an additional orthogonal loss is introduced. Thus, the overall loss term becomes  $\lambda_C \mathcal{L}_C + \lambda_{cl} \mathcal{L}_{cl} + \lambda_{sep} \mathcal{L}_{sep} + \lambda_o \mathcal{L}_o$ .

After this training step the prototypes are projected to the nearest feature vectors similar to *ProtoPNet* and the last layer is fine-tuned to optimize the classification performance.

### *PIPNet*

Nauta et al. introduced *PIPNet* [19], which incorporates two novel loss functions based on CARL (Consistent Assignment for Representation Learning) [56] to learn prototypes that more accurately align with real object parts. Unlike *ProtoPNet* or *ProtoPool*, *PIPNet* does not use explicit prototype vectors. This removes the need to project prototypes onto nearby latent patches. The architecture includes a CNN backbone (without additional convolutional layers), followed by a softmax layer and a fully connected layer. The feature map  $\mathbf{z} \in \mathcal{R}^{H \times W \times D}$  from the backbone is treated as  $D$  two-dimensional ( $H \times W$ ) prototype similarity maps. The softmax operation across the  $D$  dimension encourages a patch from the feature map  $\tilde{\mathbf{z}}_{h,w}$ , to belong to exactly one prototype similarity map. The similarity scores are again computed via a max-pooling operation and used in the fully connected layer for classification.

Unlike *ProtoPNet* and *ProtoPool*, *PIPNet* trains the entire model without fixing the last layer. To ensure positive reasoning, the fully connected layer is constrained to have only positive weights. Another key distinction is the Siamese data augmentation pipeline, where two views of the same image patch are created. These views are used in the first novel loss function, the alignment loss, that optimizes the two views to belong to the same prototype. This promotes the extraction of more general features. The second loss function, the tanh-loss, ensures that each prototype is represented at least once in a training batch to prevent trivial solutions. The last loss function is the standard classification loss. The overall loss

is defined as a linear combination of these three terms  $\lambda_C \mathcal{L}_C + \lambda_A \mathcal{L}_A + \lambda_T \mathcal{L}_T$ .

*PIPNet* follows a multistep training process. In the first step, only the backbone is optimized using the alignment and tanh loss to learn prototypes representing general, class-independent features. In the second step, the entire network is optimized using all loss terms, including classification loss. To promote sparsity during training, ensuring that each class uses a minimal number of prototypes for classification, the output scores  $o$  are calculated as follows:

$$o = \log \left( (s_m \omega_c)^2 + 1 \right) \quad (3)$$

Here,  $s_m$  are the prototype similarity scores and  $\omega_c$  the weights of the fully connected layer. The natural logarithm is employed to promote sparsity, as decreasing the weights has a higher loss gain than increasing weights when the weights become too large.

### *Multi-Label Optimization*

The *AWA2* dataset has multiple labels per image. To adapt the training objectives for this setting, we switch from a cross-entropy loss to a multi-label margin loss as the classification loss. Other common loss functions for multi-label classification include binary cross-entropy loss and multi-label soft margin loss. However, these losses tend to learn negative weights in the classification layer for labels not present in the image, which conflicts with the L1 regularization used to promote positive reasoning in the final layer. Other class specific loss functions that need to be adapted are the cluster and separation loss used in *ProtoPNet* and *ProtoPool*. We calculate the mean over the individual cluster and separation losses of each label. We argue that this simple extension remains true to the idea of these losses described in *ProtoPNet* [16].

## 4.1 Prototype Visualization

The post-hoc visualization method is not bound to the individual models, allowing us to select the most suitable method for the networks. The original implementation of *ProtoPNet* employs a simple model-agnostic upscaling method, which was also used by *ProtoPool* and *PIPNet*. This method upscales the similarity map of a prototype to the size of the input using a cubic interpolation to visualize the similarity pattern

O. Completeness	$PLC_{out} \downarrow$	$PALC_{out}\% \downarrow$	$PSC_{out}\% \downarrow$ [57]	$PRC_{out} \downarrow$ [57]	$PAC_{out}\% \downarrow$	$VLC\% \downarrow$ [57]	$VAC\% \downarrow$
Continuity	$PLC_{conti} \downarrow$	$PALC_{conti}\% \downarrow$	$PSC_{conti}\% \downarrow$	$PRC_{conti} \downarrow$	$PAC_{conti}\% \downarrow$	CAC $\downarrow$	CRC $\downarrow$
Contrastivity	$PLC_{contra} \uparrow$	$PALC_{contra}\% \uparrow$	$APD_{intra} \uparrow$	$AFD_{intra} \uparrow$	$APD_{inter} \uparrow$ [58]	$AFD_{inter} \uparrow$ [58]	Entropy $\downarrow$
C. Complexity	O. Overlap % $\downarrow$ [58]	B. Overlap % $\downarrow$	IOR $\uparrow$ [58]*	Cons. % $\uparrow$ [49]*			
Compactness	Global Size $\downarrow$ [19]	Sparsity% $\uparrow$ [19]	NPR $\downarrow$	Local Size $\downarrow$ [19]			

**Table 1** Overview of the metrics utilized, categorized by evaluation techniques, along with references to the original studies. References marked with a \* indicate that the metrics are inspired by similar metrics in this study. Down and up arrows denote the direction of improvement. Note that some metrics have variations in direction between categories. This variation arises from whether the stability of an individual prototype is assessed, whereby minimal changes are intended, or when the differences between prototypes are evaluated, which desired significant changes.

of the prototype within the image. A key disadvantage is that it relies solely on the similarity map and assumes the preservation of spatial information in the feature extraction process. There are other model-specific methods that can better visualize the feature extraction process of the model. Based on these arguments and the findings from Xu-Darme et al. [59], which compared various visualization methods, we selected the Prototypical Relevance Propagation *PRP* method from Gautam et al. [60] for visualizing the prototypes.

## 5 Evaluation Metrics

In this section, we discuss the techniques and metrics used to evaluate the part-based prototype models. Following the Co-12 properties from Nauta et al. [17] as a guideline, we choose metrics to evaluate the output-completeness, continuity, contrastivity, covariate complexity, and compactness. We use a total of 22 metrics, including 13 metrics that are novel to this domain, an overview of the metrics categorized by the evaluation techniques is shown in Table 1. We only use the top-5 most activated prototypes of a sample image to evaluate prototype quality-related metrics. This approach is aligned with the actual explanation scheme, where only a few prototypes are visualized to explain a decision to the user. To evaluate the general performance of the networks, we use accuracy, top-3 accuracy, and F1 score.

### 5.1 Output-Completeness Evaluation

The output-completeness evaluation focuses on the visualization method’s ability to highlight all relevant parts in the input image. To evaluate the output completeness of the *PRP* method, we consider the study by Sacha et al. [57], which

evaluates the spatial misalignment of visualization methods. The introduced metrics measure the location change in the visualization *VLC*, the prototype activation change *PSC*, and the prototype rank change *PRC* when a perturbation is applied to the input image. We extend this list by including the activation change of the visualization *VAC*, the location change of the maximum activation in the feature map *PLC*, as well as the general location and activation change of the similarity pattern, *PALC* and *PAC*, respectively. Some metrics from Sacha et al. [57] have been renamed for consistency in terminology.

Consider in image  $x$  and the perturbed counterpart  $\bar{x}_i$ , created based on the visualization of the prototype  $p_i \in P$ . Let  $v_{p_i}(x)$  be the saliency map of prototype  $p_i$ . Each saliency map is pre-processed and only contains pixels with a relevance value above the 95th percentile. Let  $b_{p_i}(x)$  be the bounding box around this activated region of the saliency map. Further, let  $a_{p_i}(x)$  be the similarity map and  $s_{p_i}(x)$  the similarity score of the prototype. We perturb an image  $x$  to  $\bar{x}_i$  by adding a Gaussian noise mask with a standard deviation of 0.05 to the pixels around the bounding box.

If the visualization method correctly highlights the relevant parts of the prototype, then we expect minimal changes in the model, resulting in low scores for these metrics.

The visualization location change *VLC*, previously introduced as the prototypical part location change by Sacha et al. [57], assesses the change in the location of the bounding box following a perturbation by calculating the intersection over union.

$$VLC = 1 - \frac{|b_{p_i}(x) \cap b_{p_i}(\bar{x}_i)|}{|b_{p_i}(x) \cup b_{p_i}(\bar{x}_i)|} \quad (4)$$

To evaluate the similarity change, we use the prototype similarity change *PSC*, formerly introduced

as prototype activation change by Sacha et al. [57]. This metric measures the relative change in the similarity score after the perturbation is applied.

$$PSC = \frac{|(s_{p_i}(x) - s_{p_i}(\bar{x}_i))|}{s_{p_i}(x)} \quad (5)$$

The final metric from Sacha et al. [57] is the prototype rank change *PRC*. This metric measures the prototype’s position change in the similarity score ranking of all prototypes.

$$PRC = |r_{p_i}(\bar{x}_i) - r_{p_i}(x)| \quad (6)$$

To complete the evaluation of changes in the saliency map, we introduce the visualization activation change *VAC*, which measures the change in relevance scores between two saliency maps. To be invariant to location changes in the visualization, we flatten and sort the saliency maps to get a relevance curve, represented as  $\tilde{v}_{p_i}(x)$ . The difference in activation is measured by calculating the intersection over union of the two activation curves in the following way. Let  $h \times w$  represent the height and width of the saliency map.

$$VAC = 1 - \frac{\sum_{j=1}^{h \times w} \min(\tilde{v}_{p_i}(x)_j, \tilde{v}_{p_i}(\bar{x}_i)_j)}{\sum_{j=1}^{h \times w} \max(\tilde{v}_{p_i}(x)_j, \tilde{v}_{p_i}(\bar{x}_i)_j)} \quad (7)$$

We also assess location and activation changes in the feature space using the similarity map. To measure the location change, we introduce the following two metrics. The first metric is the prototype location change *PLC*, which measures the change in the maximum activation location between two similarity maps. We will use the Manhattan distance for this measure.

$$PLC = \|\text{argmax}(a_{p_i}(x)) - \text{argmax}(a_{p_i}(\bar{x}_i))\|_1 \quad (8)$$

The other metric is the prototype activation location change *PALC*. This metric measures the location change of the hole activation pattern in the similarity map, analogous to the *VLC* metric. We apply a min-max normalization and use a threshold of 0.5 to obtain a binary activation pattern, expressed by the *bin()* operation.

$$PALC = 1 - \frac{|\text{bin}(a_{p_i}(x)) \cap \text{bin}(a_{p_i}(\bar{x}_i))|}{|\text{bin}(a_{p_i}(x)) \cup \text{bin}(a_{p_i}(\bar{x}_i))|} \quad (9)$$

To evaluate the activation change in similarity maps, we introduce the prototype activation change *PAC*, which operates similar to the *VAC* metric. Let  $m \times n$  represent the height and width of the feature map.

$$PAC = 1 - \frac{\sum_{j=1}^{m \times n} \min(a_{p_i}(x)_j, a_{p_i}(\bar{x}_i)_j)}{\sum_{j=1}^{m \times n} \max(a_{p_i}(x)_j, a_{p_i}(\bar{x}_i)_j)} \quad (10)$$

Using these additional metrics, we evaluate the changes in location and activation at each step before the final classification in the general architecture of prototype models, illustrated in Figure 1.

## 5.2 Continuity Evaluation

The continuity evaluation assesses the stability of prototypes under different augmentations. We focus on the study by Hoffmann et al. [48], which assesses prototype stability under noise and compression artifacts, and the studies by Rymarczyk et al. [33] and Nauta et al. [53], which examine the influence of photometric augmentations. We train our model using geometric and photometric augmentations to promote continuity during training, as recommended by Nauta et al. [17]. In the evaluation, we perturb the input image  $x$  to  $\bar{x}$  with photometric and noise augmentations. The individual augmentations are applied all at once with the following settings: brightness +12.5%, contrast +12.5%, saturation +12.5%, hue 0.05, noise 5%, JPEG quality 90%, and blur using a  $3 \times 3$  kernel.

We utilize the metrics from the output-completeness evaluation to evaluate the changes in location and activation within the model. The *VLC* and *VAC* scores are excluded, as they focus on assessing the visualization method instead of a prototype. We also introduce the following new metrics. The classification activation change *CAC* measures the change in prediction. Let  $K$  be the number of classes and  $o(x)$  be the output vector of the model for an image  $x$ .

$$CAC = 1 - \frac{\sum_{j=1}^K \min(o(x)_j, o(\bar{x})_j)}{\sum_{j=1}^K \max(o(x)_j, o(\bar{x})_j)} \quad (11)$$

The other metric is the classification rank change *CRC* that measures the change in the rank of

the predicted class. Let  $r_c(x)$  be the rank of the predicted class  $c$  for the image  $x$ .

$$CRC = |r_c(\bar{x}) - r_c(x)| \quad (12)$$

### 5.3 Contrastivity

The contrastivity evaluation is used to assess the differences between prototypes. To evaluate the contrastivity of prototypes, we refer to the study by Wang et al. [58], which evaluated the contrastivity of prototypes in the feature space. We follow the recommendations of Nauta et al. [17] to also assess location differences.

Wang et al. [58] measured the average cosine distance between prototypes  $APD_{inter}$  and feature vectors  $AFD_{inter}$  of different classes. These metrics are designed for networks with class-specific prototypes, so each class has a subset of prototypes  $P_k \subset P$ , where  $P$  is the set of all prototypes and  $k$  is the class index. To ensure compatibility with models that do not assign prototypes to classes, we use the ground truth class of the image  $x$  to create the subset  $P_x$ , consisting of the top-5 most activated prototypes in the image. The subset  $P_k$  is then the combination of all subsets  $P_x$  in the test set  $X_{test}$ . To create the corresponding feature vector sets  $F_k$ , we use the nearest feature vectors of the prototypes in the subset  $P_x$ .

We use the average inter-class distance metrics from Wang et al. [58] and also employ the average intra-class distance case  $APD_{intra}$  and  $AFD_{intra}$  respectively. Following the recommendations from Nauta et al. [17], we use the *PLC* and *PALC* metrics to assess the contrastivity of prototype locations in the feature map and introduce a new metric to evaluate the activation discriminativeness of prototypes.

The original study from Wang et al. [58] does not state the specific formula of the metrics, so the following calculations are our interpretation of the metrics. The average inter-class prototype distance  $APD_{inter}$  from Wang et al. [58] is the average cosine distance between prototypes of different classes and is calculated as follows:

$$APD_{inter} = \frac{1}{K} \sum_{k=1}^K \frac{1}{|P_k|} \sum_{i:p_i \in P_k} \frac{1}{|P \setminus P_k|} \cdot \sum_{j:p_j \in P \setminus P_k} \left( 1 - \frac{p_i \cdot p_j}{\|p_i\| \cdot \|p_j\|} \right) \quad (13)$$

We calculate the average inter-class feature distance  $AFD_{inter}$  from Wang et al. [58] in the same way using the feature vector set  $F$  instead of the prototype set  $P$ . To evaluate the contrastivity between prototypes from the same class, we introduce the average intra-class prototype distance  $APD_{intra}$ . The metric measures the average cosine distance of a prototype to all other prototypes of the same class and is calculated as follows:

$$APD_{intra} = \frac{1}{K} \sum_{k=1}^K \frac{1}{|P_k|} \sum_{i:p_i \in P_k} \frac{1}{|P_k \setminus p_i|} \cdot \sum_{j:p_j \in P_k \setminus p_i} \left( 1 - \frac{p_i \cdot p_j}{\|p_i\| \cdot \|p_j\|} \right) \quad (14)$$

We also extend this metric to the feature vector case introducing the average intra-class feature distance  $AFD_{intra}$ , by switching the prototype set  $P$  with the feature vector set  $F$ . To measure the class discriminativeness of a prototype, we compute the Shannon entropy of the similarity scores. Let  $S_{p_i}$  be the set of similarity scores of a prototype over all test images in  $X_{test}$ . We first use a max normalization to normalize the similarity scores and then calculate the histogram  $hist(S_{p_i})$  of the similarity scores with  $U = 10$  bins. The discriminativeness of the prototype is then calculated as follows:

$$Entropy = - \sum_{u=1}^U hist(S_{p_i})_u \cdot \log(hist(S_{p_i})_u) \quad (15)$$

A high entropy indicates that the prototype has no discriminative activation pattern.

### 5.4 Covariate Complexity

The covariate complexity evaluation assesses the complexity of a prototype regarding the interpretability. To evaluate the covariate complexity of prototypes, we focus on the study by Wang et al. [58], which evaluated the overlap of prototype visualizations with object masks, and the study by Huang et al. [49], which evaluated how consistently object parts are represented by a prototype.

The following metrics from Wang et al. [58] are again our interpretation, as the study does not provide specific formulas. To determine the activated region of a prototype in the input image,

we again use the 95th percentile approximation on the prototype visualization for these metrics.

To assess the overlap between prototypes and objects, Wang et al. [58] introduces the content heatmap metric. We renamed this metric to *Object Overlap* to be consistent with our naming scheme. The metric calculates the intersection of the prototype visualization and the object mask. Let  $m(x)$  be the object mask of image  $x$ . The metric is calculated as follows:

$$\text{Object Overlap} = \frac{|v_{p_i}(x) \cap m(x)|}{|m(x)|} \quad (16)$$

We also adapted the idea of the outside-inside relevance ratio measure from Wang et al. [58], introducing the inside-outside relevance difference *IOR* as the signed difference between mean inside and outside activation. The adoption of the original metric was made to increase the stability of the measurements. Each saliency map is normalized before the calculation to ensure that *IOR* scores are consistent between different saliency maps.

$$\text{IOR} = \frac{\sum_{j=1}^{h \times w} \tilde{v}_{p_i}(x)_j \cdot m(x)_j}{\sum_{j=1}^{h \times w} \mathbb{I}((\tilde{v}_{p_i}(x)_j \cdot m(x)_j) > 0)} - \frac{\sum_{j=1}^{h \times w} \tilde{v}_{p_i}(x)_j \cdot (1 - m(x)_j)}{\sum_{j=1}^{h \times w} \mathbb{I}((\tilde{v}_{p_i}(x)_j \cdot (1 - m(x)_j)) > 0)} \quad (17)$$

Here,  $\mathbb{I}$  is the indicator function that returns 1 if the condition is true and 0 otherwise.

To measure the alignment of prototypes with specific object parts, we adapted the consistency score from Huang et al. [49]. The coverage of an object part is calculated by computing a histogram of the object parts covered by a prototype over the test set  $X_{test}$ . This is done by computing the bounding box and adding all object parts within the bounding box to the histogram of that prototype. After processing every image in the test set, we normalize the histograms. This results in a vector with object part percentages, denoted as  $l_{p_i}$ . The consistency of the prototype is the average coverage measure over the vector  $l_{p_i}$  and is

calculated as follows:

$$\text{Consistency} = \frac{1}{|l_{p_i}|} \sum_j^{l_{p_i}} l_{p_i j} \quad (18)$$

In addition, we introduce the *Background Overlap* metric as a counterpart to the *Object Overlap*. This metric assesses the area of the activated region in the saliency map that does not overlap with the object. The metric is calculated as follows:

$$\text{Background Overlap} = 1 - \frac{|v_{p_i}(x) \cap m(x)|}{|v_{p_i}(x)|} \quad (19)$$

## 5.5 Compactness

The compactness evaluation assesses general characteristics of the model. This evaluation will focus on the study by Nauta et al. [19], which evaluated global size, local size, and the sparsity of the classification layer. Additionally, we will include the negative-positive reasoning ratio metric in our compactness evaluation.

The global explanation size from Nauta et al. [19] counts all prototypes with at least one non-zero weight in the classification layer. This definition is not directly applicable to the *ProtoPool* model. Therefore, we will count non-zero weights in the prototype presence matrix from *ProtoPool*. The local explanation size, as described by Nauta et al. [19], can be defined as follows. Let  $\hat{s}_{p_i}(x)$  be the normalized similarity score of a prototype  $p_i$  for an image  $x$ , with  $s(x)$  being the similarity score vector of all prototypes for the image  $x$ .

$$\hat{s}_{p_i}(x) = \frac{s_{p_i}(x)}{\max s(x)} \quad (20)$$

Then, we count the number of prototypes with a normalized similarity score above a threshold  $\mu$ , which is set to 0.1:

$$\text{Local Size} = \sum_{i=1}^N \mathbb{I}(\hat{s}_{p_i}(x) > 0.1) \quad (21)$$

with  $N$  as the total number of prototypes.

The classification Sparsity from Nauta et al. [19] is the ratio of zero weights in the classification layer. Let  $W$  represent the weights in the classification layer, and  $\epsilon = 0.001$  be the threshold

for considering a weight as non-zero to improve the numerical stability.

$$Sparsity = \frac{|W| - \sum_{w \in W} \mathbb{I}(w > \epsilon \vee w < -\epsilon)}{|W|} \quad (22)$$

Here,  $|W|$  denotes the total number of weights and the sum counts the number of positive and negative weights that exceed the threshold  $\epsilon$ .

To evaluate the positive reasoning property of the model, we introduce the negative-positive reasoning ratio  $NPR$ , that calculates the ratio between the number of positive and negative weights in the classification layer. We will again use a threshold of  $\epsilon = 0.001$  for considering a weight as positive or negative.

$$NPR = \frac{\sum_{w \in W} \mathbb{I}(w < -\epsilon)}{\sum_{w \in W} \mathbb{I}(w > \epsilon)} \quad (23)$$

The numerator  $\sum_{w \in W} \mathbb{I}(w < -\epsilon)$  counts the number of negative weights that are less than  $-\epsilon$ , and the denominator  $\sum_{w \in W} \mathbb{I}(w > \epsilon)$  counts the number of positive weights that are greater than  $\epsilon$ .

## 6 Experimental Setup

In this section, we briefly describe the chosen model parameters and architectural settings, as well as the dataset and training setup.

In the original studies, datasets were split into 50% training and 50% test data. We will follow a different method based on the study by Raschka et al. [61], which argues that using the same data subset for model selection and final evaluation can result in overly optimistic outcomes. Following these guidelines, we first divide the datasets into 70% training and 30% test sets. We then apply 4-fold stratified cross-validation to split the training set into training and validation subsets, maintaining a consistent class distribution across all sets. This results in four different sets of training and validation pairs, with a 52.5% training and 17.5% validation split.

We selected the *ResNet-50* architecture with pretrained ImageNet weights as a backbone for all models. The feature maps’ spatial dimensions are  $7 \times 7$ . In the original study from *PIPNet* the dimension is modified to  $28 \times 28$ . However, it is not described as a core architecture design, so we argue that the use of a uniform dimension setting

makes the comparison fairer. For the dimension of explicit prototype vectors in the *ProtoPNet* and *ProtoPool* models, we chose  $1 \times 1 \times 128$ . The last layer of *ProtoPNet* is initialized with a 1 indicating a prototype belongs to a class and 0 otherwise instead of  $-0.5$ , because the sparsity objective described by Chen et al. [16] could otherwise not be achieved in our experiments. *PIPNet* uses 2048 prototypes for all datasets. *ProtoPNet* uses 2000, 1960, 50 and 490 for *CUB200*, *Cars196*, *NICO* and *AwA2* respectively. *ProtoPool* uses 205, 201, 50, 168 prototypes for the datasets, respectively.

We used an online augmentation setting with the Albumentations library [62], that supports augmenting bounding boxes, segmentation masks, and key-points along with images, which is crucial for certain metrics in our evaluation. All networks were trained with geometric and photometric augmentations. The original studies from *ProtoPNet* and *ProtoPool* only used geometric augmentations, but due to our consistency evaluation, we choose to add additional photometric augmentations to promote better results. In the original study, the *PIPNet* model used photometric augmentation for the contrastive learning approach, which is also included in our experiments. The experiments on the *CUB200* and *Cars196* were done on cropped images using the bounding box information.

Due to the differences between our training setup and the original studies, we adjusted the learning rates, training epochs, and schedulers for each model and dataset. The new parameters were chosen based on hyperparameter tuning with 50 trails for each dataset. To reduce complexity and the computational load, we used a fixed number of 100 joint epochs to tune all models. The individual loss weights were kept the same as the original paper suggested over all datasets. All networks were re-implemented based on the original code for our experiments and are also part of our open-source library. We point out that our training setup deviates from the optimal learning procedure introduced in the original studies, and we expect a reduction in performance. Therefore, our focus is to evaluate if interpretable properties discussed in the original studies remain in suboptimal learning conditions.

CUB200	Accuracy% $\uparrow$	top-3 Acc.% $\uparrow$	F1 score% $\uparrow$	Global Size $\downarrow$	Sparsity% $\uparrow$	NPR $\downarrow$	Local Size $\downarrow$
ProtoPNet	70.18 $\pm$ 1.32	85.29 $\pm$ 0.73	70.39 $\pm$ 1.23	2000.00 $\pm$ 0.00	99.30 $\pm$ 0.18	0.25 $\pm$ 0.19	1348.02 $\pm$ 146.53
ProtoPNet P	69.12 $\pm$ 1.81	85.00 $\pm$ 0.95	69.20 $\pm$ 1.60	1891.75 $\pm$ 16.40	99.10 $\pm$ 0.38	0.19 $\pm$ 0.13	1261.84 $\pm$ 131.89
ProtoPool	67.33 $\pm$ 0.24	80.42 $\pm$ 0.96	67.81 $\pm$ 0.44	<b>205.00</b> $\pm$ 0.00	96.04 $\pm$ 0.60	0.54 $\pm$ 0.06	168.33 $\pm$ 14.58
PIPNet	<b>74.00</b> $\pm$ 0.00	<b>86.77</b> $\pm$ 0.00	<b>73.85</b> $\pm$ 0.00	858.00 $\pm$ 0.00	<b>99.31</b> $\pm$ 0.00	<b>0.00</b> $\pm$ 0.00	<b>67.69</b> $\pm$ 0.00
Cars196	Accuracy% $\uparrow$	top-3 Acc.% $\uparrow$	F1 score% $\uparrow$	Global Size $\downarrow$	Sparsity% $\uparrow$	NPR $\downarrow$	Local Size $\downarrow$
ProtoPNet	82.60 $\pm$ 1.07	94.01 $\pm$ 0.56	82.63 $\pm$ 0.99	1960.00 $\pm$ 0.00	99.35 $\pm$ 0.07	0.10 $\pm$ 0.04	1197.61 $\pm$ 106.00
ProtoPNet P	81.77 $\pm$ 0.55	93.15 $\pm$ 0.66	81.67 $\pm$ 0.46	1785.50 $\pm$ 22.78	98.78 $\pm$ 0.51	0.15 $\pm$ 0.05	1080.18 $\pm$ 84.72
ProtoPool	83.25 $\pm$ 0.57	91.62 $\pm$ 0.42	83.29 $\pm$ 0.59	<b>201.00</b> $\pm$ 0.00	99.28 $\pm$ 0.12	0.11 $\pm$ 0.07	170.47 $\pm$ 51.32
PIPNet	<b>85.78</b> $\pm$ 0.00	<b>94.68</b> $\pm$ 0.00	<b>85.73</b> $\pm$ 0.00	514.00 $\pm$ 0.00	<b>99.51</b> $\pm$ 0.00	<b>0.00</b> $\pm$ 0.00	<b>68.95</b> $\pm$ 0.00
NICO	Accuracy% $\uparrow$	top-3 Acc.% $\uparrow$	F1 score% $\uparrow$	Global Size $\downarrow$	Sparsity% $\uparrow$	NPR $\downarrow$	Local Size $\downarrow$
ProtoPNet	90.04 $\pm$ 1.30	96.74 $\pm$ 0.61	90.01 $\pm$ 1.32	<b>50.00</b> $\pm$ 0.00	60.25 $\pm$ 8.46	0.46 $\pm$ 0.12	15.59 $\pm$ 3.83
ProtoPNet P	90.19 $\pm$ 1.15	96.77 $\pm$ 0.60	90.15 $\pm$ 1.17	<b>50.00</b> $\pm$ 0.00	55.05 $\pm$ 15.82	0.51 $\pm$ 0.14	15.69 $\pm$ 3.83
ProtoPool	89.89 $\pm$ 0.92	95.94 $\pm$ 0.87	89.87 $\pm$ 0.93	<b>50.00</b> $\pm$ 0.00	89.55 $\pm$ 0.66	0.04 $\pm$ 0.07	<b>3.38</b> $\pm$ 0.83
PIPNet	<b>91.40</b> $\pm$ 0.00	<b>97.49</b> $\pm$ 0.00	<b>91.49</b> $\pm$ 0.00	214.00 $\pm$ 0.00	<b>98.90</b> $\pm$ 0.00	<b>0.00</b> $\pm$ 0.00	70.80 $\pm$ 0.00
Awa2	Accuracy% $\uparrow$	top-3 Acc.% $\uparrow$	F1 score% $\uparrow$	Global Size $\downarrow$	Sparsity% $\uparrow$	NPR $\downarrow$	Local Size $\downarrow$
ProtoPNet	43.86 $\pm$ 3.01	-	91.74 $\pm$ 0.60	490.00 $\pm$ 0.00	18.27 $\pm$ 0.95	0.95 $\pm$ 0.02	184.20 $\pm$ 17.85
ProtoPNet P	40.61 $\pm$ 8.45	-	91.75 $\pm$ 0.47	467.75 $\pm$ 7.32	18.16 $\pm$ 0.67	1.05 $\pm$ 0.13	185.56 $\pm$ 25.42
ProtoPool	46.33 $\pm$ 6.45	-	91.98 $\pm$ 1.29	<b>168.00</b> $\pm$ 0.00	96.43 $\pm$ 1.30	0.24 $\pm$ 0.29	87.76 $\pm$ 20.57
PIPNet	<b>62.41</b> $\pm$ 0.00	-	<b>94.47</b> $\pm$ 0.00	206.00 $\pm$ 0.00	<b>98.68</b> $\pm$ 0.00	<b>0.00</b> $\pm$ 0.00	<b>70.38</b> $\pm$ 0.00

**Table 2** General performance and Compactness evaluation results. The results are averaged over 4 runs with standard deviation. Training and validation subsets were created using 4-fold stratified cross-validation.

## 7 Results

The general performance, compactness, contrastivity, and continuity evaluations are conducted on all datasets. The output-completeness and complexity evaluations are conducted exclusively on the *CUB200* dataset. The output-completeness evaluation exclusively assesses the employed visualization method, in our case the computationally intensive *PRP* method; thus, this method was evaluated only on the *CUB200* dataset. The complexity evaluation is limited to the *CUB200* dataset due to the absence of object masks and part annotations in the other datasets.

The used networks are *ProtoPNet* [16], *ProtoPNet Pruned* [16], *ProtoPool* [18], and *PIPNet* [19]. The pruned version of *ProtoPNet* was created using the pruning strategy stated in the original paper.

### 7.1 General and Compactness

Table 2 presents the outcomes of our evaluations on general performance and compactness. The results obtained from *ProtoPNet* indicate that pruning adversely affects performance. The *ProtoPool* model exhibits no definitive ranking trend, frequently performing slightly worse than the *ProtoPNet* models but demonstrating an advantage

on the *Cars196* and *Awa2* datasets. The *PIPNet* model exhibits the best performance across all datasets.

Notably, all networks exhibit a considerable performance improvement when comparing overall accuracy to top-3 accuracy, showing potential gains if the models are further tuned, particularly on the fine-grained datasets *CUB200* and *Cars196*, with each containing around 200 classes. The results from the *NICO* dataset suggest that all networks are similarly influenced by the distribution shift, with no significant performance losses. Furthermore, all models show a significant performance reduction on the multi label dataset *Awa2*, suggesting that learning attributes like strides from multiple animal classes presents significant challenges. This is followed by the fine-grained datasets, where the *CUB200* dataset is more challenging than *Cars196*. In contrast, the general classification task from the *NICO* dataset appears to be the least difficult.

The compactness evaluation shows that the global size of *PIPNet* remains below its allocated number by a large margin across all datasets. *ProtoPool* could not achieve a reduction of prototypes, but uses the smallest absolute number of prototypes on all datasets, except *NICO*. The

CUB200	$PLC_{contra} \uparrow$	$PALC_{contra}\% \uparrow$	$APD_{intra} \uparrow$	$AFD_{intra} \uparrow$	$APD_{inter} \uparrow$	$AFD_{inter} \uparrow$	Entropy $\downarrow$
ProtoPNet	1.95 $\pm$ 0.28	39.83 $\pm$ 2.08	0.00 $\pm$ 0.00	0.00 $\pm$ 0.00	<b>0.01</b> $\pm$ 0.00	0.01 $\pm$ 0.00	0.99 $\pm$ 0.00
ProtoPNet P	1.92 $\pm$ 0.28	39.05 $\pm$ 2.45	0.00 $\pm$ 0.00	0.00 $\pm$ 0.00	<b>0.01</b> $\pm$ 0.00	0.01 $\pm$ 0.00	0.99 $\pm$ 0.00
ProtoPool	0.71 $\pm$ 0.06	15.60 $\pm$ 2.51	0.00 $\pm$ 0.00	0.00 $\pm$ 0.00	0.00 $\pm$ 0.00	0.00 $\pm$ 0.00	0.91 $\pm$ 0.01
PIPNet	<b>3.99</b> $\pm$ 0.06	<b>100.00</b> $\pm$ 0.00	-	<b>1.00</b> $\pm$ 0.00	-	<b>0.96</b> $\pm$ 0.00	<b>0.34</b> $\pm$ 0.01
Cars196	$PLC_{contra} \uparrow$	$PALC_{contra}\% \uparrow$	$APD_{intra} \uparrow$	$AFD_{intra} \uparrow$	$APD_{inter} \uparrow$	$AFD_{inter} \uparrow$	Entropy $\downarrow$
ProtoPNet	2.02 $\pm$ 0.15	59.82 $\pm$ 3.26	0.00 $\pm$ 0.00	0.00 $\pm$ 0.00	<b>0.02</b> $\pm$ 0.00	0.02 $\pm$ 0.00	0.96 $\pm$ 0.01
ProtoPNet P	1.94 $\pm$ 0.10	58.40 $\pm$ 2.35	0.00 $\pm$ 0.00	0.00 $\pm$ 0.00	<b>0.02</b> $\pm$ 0.00	0.02 $\pm$ 0.00	0.96 $\pm$ 0.01
ProtoPool	1.69 $\pm$ 0.88	40.94 $\pm$ 21.70	<b>0.01</b> $\pm$ 0.00	0.01 $\pm$ 0.00	0.01 $\pm$ 0.01	0.01 $\pm$ 0.01	0.86 $\pm$ 0.05
PIPNet	<b>4.00</b> $\pm$ 0.04	<b>100.00</b> $\pm$ 0.00	-	<b>1.00</b> $\pm$ 0.00	-	<b>0.99</b> $\pm$ 0.00	<b>0.35</b> $\pm$ 0.00
NICO	$PLC_{contra} \uparrow$	$PALC_{contra}\% \uparrow$	$APD_{intra} \uparrow$	$AFD_{intra} \uparrow$	$APD_{inter} \uparrow$	$AFD_{inter} \uparrow$	Entropy $\downarrow$
ProtoPNet	1.56 $\pm$ 0.27	45.71 $\pm$ 7.30	0.00 $\pm$ 0.00	0.00 $\pm$ 0.00	0.03 $\pm$ 0.00	0.03 $\pm$ 0.00	0.54 $\pm$ 0.04
ProtoPNet P	1.55 $\pm$ 0.26	45.64 $\pm$ 7.21	0.00 $\pm$ 0.00	0.00 $\pm$ 0.00	0.03 $\pm$ 0.00	0.03 $\pm$ 0.00	0.53 $\pm$ 0.04
ProtoPool	1.46 $\pm$ 0.10	34.37 $\pm$ 4.21	<b>0.10</b> $\pm$ 0.02	0.03 $\pm$ 0.01	<b>0.13</b> $\pm$ 0.02	0.16 $\pm$ 0.01	0.75 $\pm$ 0.11
PIPNet	<b>3.86</b> $\pm$ 0.05	<b>100.00</b> $\pm$ 0.00	-	<b>1.00</b> $\pm$ 0.00	-	<b>0.97</b> $\pm$ 0.01	<b>0.35</b> $\pm$ 0.00
AWA2	$PLC_{contra} \uparrow$	$PALC_{contra}\% \uparrow$	$APD_{intra} \uparrow$	$AFD_{intra} \uparrow$	$APD_{inter} \uparrow$	$AFD_{inter} \uparrow$	Entropy $\downarrow$
ProtoPNet	3.86 $\pm$ 0.44	85.06 $\pm$ 2.72	0.01 $\pm$ 0.00	0.01 $\pm$ 0.00	-	-	0.88 $\pm$ 0.03
ProtoPNet P	3.87 $\pm$ 0.40	86.10 $\pm$ 2.66	0.01 $\pm$ 0.00	0.01 $\pm$ 0.00	-	-	0.90 $\pm$ 0.03
ProtoPool	2.87 $\pm$ 1.02	22.96 $\pm$ 3.57	<b>0.04</b> $\pm$ 0.03	0.04 $\pm$ 0.03	-	-	0.85 $\pm$ 0.05
PIPNet	<b>3.74</b> $\pm$ 0.02	<b>100.00</b> $\pm$ 0.00	-	<b>1.00</b> $\pm$ 0.00	-	-	<b>0.32</b> $\pm$ 0.00

**Table 3** Contrastivity evaluation results. The results are averaged over 4 runs with standard deviation. Training and validation subsets were created using 4-fold stratified cross-validation.

pruning method employed by *ProtoPNet* consistently reduces the global size of the original model by a small margin, except on the *NICO* dataset.

The sparsity results reveal that only *PIPNet* achieves consistent results on all datasets. The results of other models fluctuate, indicating dataset and task dependencies.

We see that the *ProtoPNet* models do not achieve a satisfactory degree of sparsity on the multi-label classification task (*AWA2*). The sparsity on the general classification task (*NICO*) is also significantly lower compared to other models. *ProtoPool* shows only a noticeably lowered sparsity on the *NICO* dataset. The pruning of the *ProtoPNet* models reduces sparsity by a small margin. This indicates that the deleted prototypes are associated with fewer classes in the classification layer compared to the retained prototypes, which is an unexpected finding. The pruning strategy calculates prototype-class pairs based on the distance to feature vectors and retains prototypes that have a clear class assignment. Prototypes retained should, therefore, also display a clearer assignment within the classification layer than the deleted ones.

*PIPNet* consistently achieves a perfect *NPR* score due to its hard constraint that ensures only

positive weights in the classification layer. The pruning of *ProtoPNet* reduces the local size of the model on the fine-grained classification tasks, indicating that the deleted prototypes were present in a notable portion of the test images. *ProtoPool* only achieves the best local size results on the *NICO* dataset despite the small global size, suggesting that the learned prototypes are complex representations without a clear class correspondence in the other datasets. *PIPNet* consistently achieves one of the best local size results, except for the *NICO* dataset. The similar results across tasks and datasets suggest that *PIPNet*'s local size is mostly dependent on the initial number of prototypes.

## 7.2 Contrastivity

The results from the contrastivity evaluation are presented in Table 3. Here, we compared the top-5 most activated prototypes of an image. To increase understanding, some metrics have been labelled with an additional subscript to indicate their different meanings across sections.

*PIPNet* repeatedly achieves the highest  $PALC_{contra}$  score across all datasets. Its  $PLC_{contra}$  score is also consistently the highest. A perfect  $PALC_{contra}$  score for *PIPNet* indicates that the

architecture design employed in combination with the loss functions is very effective in learning focused prototype activations without any overlap with other prototypes. In contrast, the lower  $PALC_{contra}$  scores in other models show their prototype activations are more dispersed. *ProtoPool* has the lowest  $PALC_{contra}$  score on all datasets, suggesting that its focused similarity approach was unsuccessful in preventing overlapping activation patterns. A low contrast between prototypes is further confirmed by the low  $PLC_{contra}$  scores, showing that the maximum activations are also close to each other.

*PIPNet* does not have explicit prototype vectors, rendering the prototype distance metrics inapplicable. However, the feature distances of the *PIPNet* models exhibit nearly perfect results after the softmax layer of the model. In the *AWA2* dataset’s multi-label setting, measuring vector distances between labels is also unfeasible due to the 1: $n$  relation between sample images and labels. The other models could not learn a reasonable distinction between prototypes on all datasets. This indicates that the contrastivity between classes is learned differently.

Entropy results show that *PIPNet* exhibits the least fluctuation in similarity scores of individual prototypes on all datasets. This contrasts with our expectation that prototypes shared among classes should have a higher fluctuation. Furthermore, despite the general low performance on the *AWA2* dataset, *PIPNet* retained its low entropy score in comparison to the other models, indicating that the model architecture actively facilitates the learning of distinct prototype activations. The entropy results from the other models are notably higher. Especially, results on the fine-grained and the *AWA2* dataset show high entropy values, indicating a correlation with the overall difficulty of the tasks. In general, the architecture of the other models do not actively promote class distinct prototype activations.

### 7.3 Continuity

The continuity evaluation measures the change of a single prototype when augmentations are applied on the input image. We will again use the top-5 most activated prototypes per image. To distinguish the continuity results shown in Table 4

from other sections, we have added subscripts to some metrics.

*PIPNet* consistently achieves the lowest  $PLC_{conti}$  and  $PALC_{conti}$  scores across all datasets by a considerable margin, suggesting that the prototype locations remain robust against applied augmentations. The comparison of  $PLC_{conti}$  and  $PALC_{conti}$  scores among other models shows that *ProtoPNet* achieves better results on the fine-grained datasets, and *ProtoPool* shows no distinct performance correlation across tasks.

Furthermore, *PIPNet* achieves significantly better  $PSC_{conti}$  and  $PAC_{conti}$  scores on all datasets. This indicates that the model design enhances the robustness of extracted features against augmentations compared to other models. We can also see that the pruning of the *ProtoPNet* models does not adversely impact these metrics. Indicating that the remaining prototypes have similar continuity properties compared to the deleted prototypes.

There is no clear trend when comparing  $PSC_{conti}$  and  $PRC_{conti}$  scores, which may initially seem counterintuitive, as we would expect that smaller changes in the similarity score would also stabilize the ranking of these scores. In contrast, the results indicate a strong model dependency. *PIPNet* shows near-perfect similarity score and rank stability on all datasets. *ProtoPool* achieves better rank stability compared to their  $PSC_{conti}$  performance, and *ProtoPNet* displays the reverse case.

$CRC$  scores show that classification accuracy is influenced by augmentations across all models, with *PIPNet* demonstrating higher robustness in the classification process. We see similar  $CAC$  performance on the fine-grained datasets. However, *ProtoPNet* shows increased classification activation fluctuation on the other datasets. Again, there is no clear correlation between  $CAC$  and  $CRC$  similar to the observations between  $PSC_{conti}$  and  $PRC_{conti}$  scores.

Comparing the  $CAC$  and  $PSC_{conti}$  scores does not reveal a clear correlation between changes in similarity scores and prediction scores. This indicates a complex relationship between prototypes and classes, which reduces the interpretability of the classification process.

CUB200	$PLC_{conti} \downarrow$	$PSC_{conti}\% \downarrow$	$PRC_{conti} \downarrow$	$PALC_{conti}\% \downarrow$	$PAC_{conti}\% \downarrow$	CAC $\downarrow$	CRC $\downarrow$
ProtoPNet	1.20 $\pm$ 0.14	16.93 $\pm$ 1.18	10.88 $\pm$ 3.94	34.42 $\pm$ 1.80	14.09 $\pm$ 1.17	6.35 $\pm$ 0.58	1.87 $\pm$ 0.25
ProtoPNet P	1.20 $\pm$ 0.16	16.98 $\pm$ 1.06	9.79 $\pm$ 3.47	34.20 $\pm$ 1.87	14.16 $\pm$ 1.09	<b>6.34</b> $\pm$ 0.59	1.72 $\pm$ 0.17
ProtoPool	2.64 $\pm$ 0.26	49.31 $\pm$ 9.99	2.38 $\pm$ 0.17	39.52 $\pm$ 4.08	17.34 $\pm$ 0.97	6.71 $\pm$ 0.17	3.70 $\pm$ 0.36
PIPNet	<b>0.05</b> $\pm$ 0.00	<b>0.47</b> $\pm$ 0.09	<b>0.94</b> $\pm$ 0.04	<b>2.89</b> $\pm$ 0.24	<b>3.82</b> $\pm$ 0.40	6.49 $\pm$ 0.17	<b>0.34</b> $\pm$ 0.04
Cars196	$PLC_{conti} \downarrow$	$PSC_{conti}\% \downarrow$	$PRC_{conti} \downarrow$	$PALC_{conti}\% \downarrow$	$PAC_{conti}\% \downarrow$	CAC $\downarrow$	CRC $\downarrow$
ProtoPNet	0.79 $\pm$ 0.06	20.55 $\pm$ 1.15	9.77 $\pm$ 1.32	33.54 $\pm$ 2.40	14.18 $\pm$ 0.75	5.84 $\pm$ 0.38	0.58 $\pm$ 0.04
ProtoPNet P	0.78 $\pm$ 0.05	20.15 $\pm$ 0.99	8.20 $\pm$ 0.77	32.82 $\pm$ 2.16	14.16 $\pm$ 0.73	5.88 $\pm$ 0.37	0.62 $\pm$ 0.07
ProtoPool	1.22 $\pm$ 0.36	34.92 $\pm$ 41.02	6.44 $\pm$ 3.36	34.28 $\pm$ 15.10	17.28 $\pm$ 7.19	<b>5.11</b> $\pm$ 0.45	1.36 $\pm$ 0.14
PIPNet	<b>0.01</b> $\pm$ 0.00	<b>0.05</b> $\pm$ 0.01	<b>0.77</b> $\pm$ 0.03	<b>0.82</b> $\pm$ 0.09	<b>0.98</b> $\pm$ 0.09	5.68 $\pm$ 0.50	<b>0.13</b> $\pm$ 0.01
NICO	$PLC_{conti} \downarrow$	$PSC_{conti}\% \downarrow$	$PRC_{conti} \downarrow$	$PALC_{conti}\% \downarrow$	$PAC_{conti}\% \downarrow$	CAC $\downarrow$	CRC $\downarrow$
ProtoPNet	1.83 $\pm$ 0.15	58.56 $\pm$ 6.43	2.23 $\pm$ 0.13	54.81 $\pm$ 3.41	26.15 $\pm$ 2.12	27.03 $\pm$ 1.66	0.28 $\pm$ 0.04
ProtoPNet P	1.82 $\pm$ 0.15	58.90 $\pm$ 6.71	2.22 $\pm$ 0.11	54.84 $\pm$ 3.37	26.21 $\pm$ 2.09	27.05 $\pm$ 1.65	0.27 $\pm$ 0.03
ProtoPool	1.43 $\pm$ 0.15	51.71 $\pm$ 5.35	<b>1.02</b> $\pm$ 0.21	31.37 $\pm$ 1.23	18.12 $\pm$ 2.20	16.42 $\pm$ 2.70	0.36 $\pm$ 0.06
PIPNet	<b>0.02</b> $\pm$ 0.01	<b>0.30</b> $\pm$ 0.10	1.34 $\pm$ 0.12	<b>0.81</b> $\pm$ 0.41	<b>1.32</b> $\pm$ 0.56	<b>11.05</b> $\pm$ 0.50	<b>0.08</b> $\pm$ 0.01
AwA2	$PLC_{conti} \downarrow$	$PSC_{conti}\% \downarrow$	$PRC_{conti} \downarrow$	$PALC_{conti}\% \downarrow$	$PAC_{conti}\% \downarrow$	CAC $\downarrow$	CRC $\downarrow$
ProtoPNet	1.48 $\pm$ 0.16	57.46 $\pm$ 2.10	5.09 $\pm$ 0.72	47.01 $\pm$ 2.03	15.60 $\pm$ 0.52	8.24 $\pm$ 0.54	-
ProtoPNet P	1.46 $\pm$ 0.15	56.61 $\pm$ 2.61	5.23 $\pm$ 0.43	46.30 $\pm$ 2.29	15.35 $\pm$ 0.70	8.68 $\pm$ 0.47	-
ProtoPool	2.43 $\pm$ 0.64	10.05 $\pm$ 3.49	1.45 $\pm$ 0.10	22.35 $\pm$ 7.69	13.47 $\pm$ 2.79	4.02 $\pm$ 0.30	-
PIPNet	<b>0.00</b> $\pm$ 0.00	<b>0.11</b> $\pm$ 0.01	<b>1.34</b> $\pm$ 0.03	<b>0.01</b> $\pm$ 0.01	<b>0.16</b> $\pm$ 0.02	<b>3.79</b> $\pm$ 0.17	-

**Table 4** Continuity evaluation results. The results are averaged over 4 runs with standard deviation. Training and validation subsets were created using 4-fold stratified cross-validation.

## 7.4 Output-Completeness and Covariate Complexity

The results of the Output-Completeness and Covariate Complexity evaluation on the *CUB200* dataset are presented in Table 5. The Output-Completeness evaluation measures the change of a single prototype, akin to the continuity evaluation. However, the augmentation is derived from the *PRP* visualization method. Again, we used the top-5 most activated prototypes per image. Subscripts have been added to metrics that were also used in the previous evaluations.

*PIPNet* consistently achieves the lowest scores across all metrics evaluating the latent space, often by a significant margin, suggesting that prototype activations in the latent space closely correspond to prototype visualizations in the input space. This stands in contrast with the *VLC* and *VAC* scores validating the accuracy of the *PRP* method, in which the *PIPNet* model exhibits results comparable to those of the other models. This indicates that the *PRP* method is generally influenced by noise augmentations of irrelevant pixels.

Comparing the original *ProtoPNet* model to its pruned variant, we can again observe comparable performance. *ProtoPool* exhibits similar changes in visualization, as shown by the *VLC* and

*VAC* scores. However, the *ProtoPool* model shows notable higher changes in the latent space. This is unexpected considering that the *PRP* method starts at the maximum activation to backpropagate relevance scores. Changes in the maximum location measured with  $PLC_{out}$  should result in more drastic changes in the input space. This is an indication that the feature vectors in the latent space are not well separated.

An *IORD* score near zero indicates a similar mean activation inside and outside the object. This suggests that the most important image regions of individual prototypes typically correspond to the object contour lines. This can be seen in Figure 2 in the example images from the *CUB200* dataset. However, it is also evident that slightly negative scores are a direct indicator that prototypes focus more on the background, measured by the *Background Overlap*.

*Object Overlap* scores suggest that the learned prototypes across all networks predominantly focus on individual parts of the object, as intended. Notably, *ProtoPool* exhibits the smallest overlap, indicating that its prototypes are the most focused. However, the measured *Background Overlap* indicates that a significant portion of the prototype activations from *ProtoPool* is directed towards the background,

Completeness	VLC% ↓	VAC% ↓	$PLC_{out}$ ↓	$PSC_{out}$ % ↓	$PRC_{out}$ ↓	$PALC_{out}$ % ↓	$PAC_{out}$ % ↓
ProtoPNet	<b>42.77</b> ± 1.18	9.17 ± 1.17	0.24 ± 0.04	3.70 ± 0.31	0.84 ± 0.06	46.49 ± 1.87	4.76 ± 0.11
ProtoPNet P	42.89 ± 1.03	9.13 ± 1.19	0.25 ± 0.04	3.67 ± 0.31	0.78 ± 0.05	47.56 ± 1.36	4.75 ± 0.12
ProtoPool	44.90 ± 0.83	9.38 ± 0.80	1.73 ± 0.26	43.97 ± 11.10	1.32 ± 0.14	95.48 ± 1.37	10.16 ± 1.39
PIPNet	43.47 ± 0.45	<b>5.75</b> ± 0.21	<b>0.01</b> ± 0.00	<b>0.03</b> ± 0.01	<b>0.16</b> ± 0.00	<b>0.43</b> ± 0.08	<b>0.59</b> ± 0.06
Complexity	Object Overlap %	Background Overlap % ↓	IODR ↑	Consistency % ↑	-	-	-
ProtoPNet	10.33 ± 1.64	24.70 ± 11.79	<b>0.03</b> ± 0.03	42.83 ± 3.27			
ProtoPNet P	10.49 ± 1.57	<b>23.63</b> ± 11.21	<b>0.03</b> ± 0.03	43.32 ± 4.46			
ProtoPool	1.98 ± 0.37	84.79 ± 2.71	-0.06 ± 0.01	42.17 ± 2.76			
PIPNet	5.25 ± 0.03	60.37 ± 0.29	-0.02 ± 0.00	<b>48.39</b> ± 1.04			

**Table 5** Output-Completeness and Complexity evaluation results on the CUB-200-2011 dataset. The results are averaged over 4 runs with standard deviation. Training and validation subsets were created using 4-fold stratified cross-validation.

thereby rendering the assumption of focused prototypes ambiguous. The results from the *ProtoPNet* models show that the pruning strategy could not lower the *Background Overlap* metric significantly. This suggests that the learned prototypes are complex mixtures of object and background that cannot easily be split into these two groups.

*PIPNet* has the highest *Consistency* score, supporting the architectural intention to enhance the semantic alignment of prototypes with object parts relative to prior models. The pruning of *ProtoPNet* has only slight effects on the *Consistency*, again suggesting that prototypes are a complex mixture of object and background, which makes it difficult to prune a specific subset.

Overall *Consistency* scores remain comparatively low, suggesting that prototypes generally do not align with individual object parts. This significantly affects interpretability, given that the primary objective of these networks is to represent distinct features with prototypes.

## 8 Discussion

In comparison with the results presented in the original papers, we find that the performance of our *PIPNet* models is approximately 8% lower than those reported by Nauta et al. [19]. We attribute this notable difference to the change in feature map resolution from  $28 \times 28$  in the original paper to  $7 \times 7$  used in our experiments to ensure a more equal comparison. The *ProtoPNet* and *ProtoPool* results exhibit a decrease of approximately 5% to 10% in the *CUB200* and *Cars196* datasets compared to the original paper. We attribute these differences primarily to the prototype channel reduction from 256 to 128, due to unstable performance results with the original channel configuration in our training setup and

the imbalanced class distribution within our training set. Although class weights were employed in the classification loss to encourage equal learning across classes, cluster loss and separation loss were not similarly weighted. The original *ProtoPNet* and *ProtoPool* models were trained with an offline augmentation approach, which balanced the class distribution before training, making the use of weights unnecessary. Evaluating on a separate test set that was not utilized for selecting the best-performing model also generally results in a slight reduction in accuracy.

No comparable results exist for the *NICO* dataset. With performance approaching 90%, we conclude that prototype models exhibit general robustness to distribution shifts.

The performance of our *AWA2* results ranges from 40% to 62%, with *PIPNet* demonstrating the highest performance and *ProtoPNet Pruned* the lowest. The relatively low performance across all models indicates that extracting understandable features is a challenging task for these models. Despite the frequently cited characterization of prototypes as general, interpretable features, the results from the *AWA2* dataset demonstrate that there is substantial room for improvement in this context. We also acknowledge that performance can be further improved due to our inability to apply class weights in the classification loss despite a highly imbalanced label distribution, given that the applied multi-label margin loss does not accommodate this.

The compactness results from *PIPNet* indicate comparable reductions in global size while exhibiting high sparsity in the classification layer, supporting the findings reported in the original paper by Nauta et al. [19]. The results from *ProtoPNet* did not clearly verify the effects of pruning as discussed by Chen et al. [16], as seen by

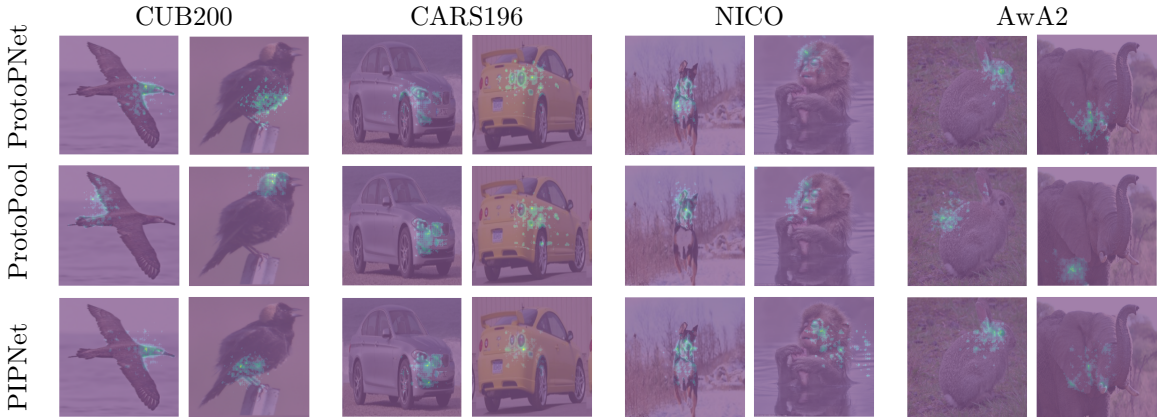


**Fig. 2** Prototype saliency maps using the PRP visualization method. The visualized prototype is the most activated on the respective image. Each saliency map visualizes only the 95th percentile.

the marginal improvement of *Background Overlap*. Comparing the *NPR* scores, it is evident that the non-negative classification layer of *PIPNet* is the only robust approach that guarantees positive reasoning among the models. Considering the sparsity and local size results, we conclude that *PIPNet* exhibits the highest interpretability in the classification layer.

The contrastivity results exhibit a similar pattern. *PIPNet* attains some of the highest results across the majority of metrics. Notably, the unique prototype locations without any overlap with other prototypes represent a significant improvement in interpretability over the other models. When we focus on the learned feature space, *PIPNet* shows well separated feature vectors underlying the effectiveness of the design. The other networks could not learn a meaningful latent space. This indicates that a well separated latent space is not robust to changing training setups.

The continuity evaluation demonstrates that *PIPNet* generally exhibits the most stable prototype locations and similarity scores, indicating that the network extracts stable high-level features rather than basic image characteristics. The other models frequently exhibit inferior results, suggesting that the contrastive learning strategy employed by *PIPNet* actively facilitates the extraction of high-level features.

In comparing the individual results of our output-completeness experiments, the *PRP* method exhibits a high degree of alignment with the subset of relevant pixels for a prototype within the *PIPNet* model. The other models exhibit

inferior performance, suggesting that the *PRP* method is significantly influenced by the learned feature extraction. It can be argued that the learned feature extraction does not necessarily ensure the spatial alignment of the feature map with the input image. This suggests that visualizations can be enhanced by utilizing more sophisticated methods such as *PRP* rather than relying on the original upsampling method, which requires the spatial alignment between the feature map and the input image.

Wang et al. [58] report that the *ProtoPNet* model using the original upsampling visualization method achieves significantly higher *Object Overlap* measures on the *CUB200* dataset. A visual comparison of the methods reveals that the upsampling method typically produces larger activation regions in the visualizations than the *PRP* method, thereby confirming these findings. The typical *PRP* visualization is illustrated in Figure 2, where the *PRP* saliency maps consist of multiple small regions.

The consistency results indicate that the prototypes are generally misaligned with specific object parts across the test set. Nauta et al. [19] introduced a purity metric to measure such alignment using the 10 most similar images to a prototype in the training set, where *PIPNet*'s prototypes achieve such an object-part alignment. Our consistency metric assigns an image to a prototype if it ranks among the top-5 most similar prototypes. Considering that the average local size of *PIPNet* is notably higher than 5, which implies that the prototypes in the top-5 exhibit reasonable

similarity to the image. The results suggest that *PIPNet*'s object-part alignment decreases significantly in the absence of near-perfect similarity scores, which can only be observed in the 10 most similar images from the training set.

## 9 Conclusion

We examined the evaluation of prototype-based neural networks, drawing on the foundational research by Nauta and Seifert [17] and Nauta et al. [63]. The Co-12 properties identified by Nauta et al. [63] provide a robust framework for assessing the quality of explanations in XAI methods. We complement these using several new metrics and provide a comprehensive evaluation using four datasets. Our python library integrates the existing evaluation techniques in the Co-12 framework and offers a practical toolkit for validating, benchmarking, and comparing part-based prototype networks.

For future work, we aim to apply this library for developing and refining new prototype models, in particular for (fine-)tuning and evaluation. In addition, we aim to extend the experimentation on further datasets.

## Statements and Declarations

All authors certify that they have no affiliations with or involvement in any organization or entity with any financial interest or non-financial interest in the subject matter or materials discussed in this manuscript.

## Acknowledgments

This work has been partially supported by the funded project FRED, German Federal Ministry for Economic Affairs and Climate Action (BMWK), FKZ: 01MD22003E, as well as by the German Research Foundation (DFG), grant MODUS-II (316679917, AT 88/4-2).

## References

- [1] Xizhao Wang, Yanxia Zhao, and Farhad Pourpanah. Recent advances in deep learning. *International Journal of Machine Learning and Cybernetics*, 11:747–750, 2020.
- [2] Samira Pouyanfar, Saad Sadiq, Yilin Yan, Haiman Tian, Yudong Tao, Maria Presa Reyes, Mei-Ling Shyu, Shu-Ching Chen, and Sundaraja S Iyengar. A survey on deep learning: Algorithms, techniques, and applications. *ACM computing surveys (CSUR)*, 51(5):1–36, 2018.
- [3] Cynthia Rudin, Chaofan Chen, Zhi Chen, Haiyang Huang, Lesia Semenova, and Chudi Zhong. Interpretable machine learning: Fundamental principles and 10 grand challenges. *Statistic Surveys*, 16:1–85, 2022.
- [4] Mengnan Du, Ninghao Liu, and Xia Hu. Techniques for interpretable machine learning. *Communications of the ACM*, 63(1):68–77, 2019.
- [5] Yu Zhang, Peter Tiño, Aleš Leonardis, and Ke Tang. A survey on neural network interpretability. *IEEE Transactions on Emerging Topics in Computational Intelligence*, 5(5):726–742, 2021.
- [6] Martin Atzmueller, Johannes Fürnkranz, Tomáš Kliegr, and Ute Schmid. Explainable and interpretable machine learning and data mining. *Data Mining and Knowledge Discovery*, 38(5):2571–2595, 2024.
- [7] Cynthia Rudin. Stop explaining black box machine learning models for high stakes decisions and use interpretable models instead. *Nature machine intelligence*, 1(5):206–215, 2019.
- [8] Gregor Stiglic, Primoz Kocbek, Nino Fijacko, Marinka Zitnik, Katrien Verbert, and Leona Cilar. Interpretability of machine learning-based prediction models in healthcare. *Wiley Interdisciplinary Reviews: Data Mining and Knowledge Discovery*, 10(5):e1379, 2020.
- [9] Martin Atzmueller. Declarative aspects in explicative data mining for computational sensemaking. In *Proc. International Conference on Declarative Programming*, pages 97–114. Springer, 2017.
- [10] Scott M Lundberg and Su-In Lee. A unified approach to interpreting model predictions. In I. Guyon, U. Von Luxburg, S. Bengio, H. Wallach, R. Fergus, S. Vishwanathan, and R. Garnett, editors, *Advances in Neural Information Processing Systems*, volume 30. Curran Associates, Inc., 2017.
- [11] Marco Tulio Ribeiro, Sameer Singh, and Carlos Guestrin. "Why should i trust you?"

- Explaining the predictions of any classifier. In *Proc. ACM SIGKDD*, pages 1135–1144, 2016.
- [12] Zhongang Qi, Saeed Khorrarn, and Fuxin Li. Visualizing deep networks by optimizing with integrated gradients. In *CVPR workshops*, volume 2, pages 1–4, 2019.
- [13] Ramprasaath R Selvaraju, Michael Cogswell, Abhishek Das, Ramakrishna Vedantam, Devi Parikh, and Dhruv Batra. Grad-cam: visual explanations from deep networks via gradient-based localization. *International journal of computer vision*, 128:336–359, 2020.
- [14] Julius Adebayo, Justin Gilmer, Michael Muelly, Ian Goodfellow, Moritz Hardt, and Been Kim. Sanity checks for saliency maps. *Advances in neural information processing systems*, 31, 2018.
- [15] Oscar Li, Hao Liu, Chaofan Chen, and Cynthia Rudin. Deep learning for case-based reasoning through prototypes: A neural network that explains its predictions. *Proc. AAAI Conference on Artificial Intelligence*, 32(1), Apr. 2018.
- [16] Chaofan Chen, Oscar Li, Daniel Tao, Alina Barnett, Cynthia Rudin, and Jonathan K Su. This looks like that: deep learning for interpretable image recognition. *Advances in neural information processing systems*, 32, 2019.
- [17] Meike Nauta and Christin Seifert. The co-12 recipe for evaluating interpretable part-prototype image classifiers. In *World Conference on Explainable Artificial Intelligence*, pages 397–420. Springer, 2023.
- [18] Dawid Rymarczyk, Łukasz Struski, Michał Górszczak, Koryna Lewandowska, Jacek Tabor, and Bartosz Zieliński. Interpretable image classification with differentiable prototypes assignment. In *European Conference on Computer Vision*, pages 351–368. Springer, 2022.
- [19] Meike Nauta, Jörg Schlötterer, Maurice Van Keulen, and Christin Seifert. Pip-net: Patch-based intuitive prototypes for interpretable image classification. In *Proc. IEEE/CVF Conference on Computer Vision and Pattern Recognition*, pages 2744–2753, 2023.
- [20] Catherine Wah, Steve Branson, Peter Welinder, Pietro Perona, and Serge Belongie. The caltech-ucsd birds-200-2011 dataset. 2011.
- [21] Jonathan Krause, Michael Stark, Jia Deng, and Li Fei-Fei. 3d object representations for fine-grained categorization. In *Proc. IEEE international conference on computer vision workshops*, pages 554–561, 2013.
- [22] Yue He, Zheyang Shen, and Peng Cui. Towards non-iid image classification: A dataset and baselines. *Pattern Recognition*, 110:107383, 2021.
- [23] Yongqin Xian, Christoph H Lampert, Bernt Schiele, and Zeynep Akata. Zero-shot learning—a comprehensive evaluation of the good, the bad and the ugly. *IEEE transactions on pattern analysis and machine intelligence*, 41(9):2251–2265, 2018.
- [24] Michael Biehl, Barbara Hammer, and Thomas Villmann. Prototype-based models in machine learning. *Wiley Interdisciplinary Reviews: Cognitive Science*, 7(2):92–111, 2016.
- [25] Roger C Schank. The structure of episodes in memory. In *Representation and understanding*, pages 237–272. Elsevier, 1975.
- [26] Janet L Kolodner. An introduction to case-based reasoning. *Artificial intelligence review*, 6(1):3–34, 1992.
- [27] Frode Sørmo, Jörg Cassens, and Agnar Aamodt. Explanation in case-based reasoning—perspectives and goals. *Artificial Intelligence Review*, 24:109–143, 2005.
- [28] Eleonora Poeta, Gabriele Ciravegna, Eliana Pastor, Tania Cerquitelli, and Elena Baralis. Concept-based explainable artificial intelligence: A survey. *arXiv preprint arXiv:2312.12936*, 2023.
- [29] Pang Wei Koh, Thao Nguyen, Yew Siang Tang, Stephen Mussmann, Emma Pierson, Been Kim, and Percy Liang. Concept bottleneck models. In Hal Daumé III and Aarti Singh, editors, *Proc. 37th International Conference on Machine Learning*, volume 119 of *Proceedings of Machine Learning Research*, pages 5338–5348. PMLR, 13–18 Jul 2020.
- [30] Been Kim, Martin Wattenberg, Justin Gilmer, Carrie Cai, James Wexler, Fernanda Viegas, et al. Interpretability beyond feature attribution: Quantitative testing with concept activation vectors (tcav). In *International conference on machine learning*, pages 2668–2677. PMLR, 2018.

- [31] Jiaqi Wang, Huafeng Liu, Xinyue Wang, and Liping Jing. Interpretable image recognition by constructing transparent embedding space. In *Proc. IEEE/CVF International Conference on Computer Vision (ICCV)*, pages 895–904, 2021.
- [32] Meike Nauta, Ron Van Bree, and Christin Seifert. Neural prototype trees for interpretable fine-grained image recognition. In *Proc. IEEE/CVF conference on computer vision and pattern recognition*, pages 14933–14943, 2021.
- [33] Dawid Rymarczyk, Łukasz Struski, Jacek Tabor, and Bartosz Zieliński. Protopshare: Prototypical parts sharing for similarity discovery in interpretable image classification. In *Proc. ACM SIGKDD, KDD '21*, page 1420–1430, New York, NY, USA, 2021. ACM. ISBN 9781450383325.
- [34] Mengqi Xue, Qihan Huang, Haofei Zhang, Lechao Cheng, Jie Song, Minghui Wu, and Mingli Song. Protopformer: Concentrating on prototypical parts in vision transformers for interpretable image recognition. *arXiv preprint arXiv:2208.10431*, 2022.
- [35] Yao Ming, Panpan Xu, Huamin Qu, and Liu Ren. Interpretable and steerable sequence learning via prototypes. In *Proc. ACM SIGKDD*, pages 903–913, 2019.
- [36] Zaixi Zhang, Qi Liu, Hao Wang, Chengqiang Lu, and Cheekong Lee. Protgnn: Towards self-explaining graph neural networks. In *Proc. AAAI Conference on Artificial Intelligence*, volume 36, pages 9127–9135, 2022.
- [37] Mikołaj Sacha, Dawid Rymarczyk, Łukasz Struski, Jacek Tabor, and Bartosz Zieliński. Protoseg: Interpretable semantic segmentation with prototypical parts. In *Proc. IEEE/CVF Winter Conference on Applications of Computer Vision (WACV)*, pages 1481–1492, January 2023.
- [38] Srishti Gautam, Ahcène Boubekki, Stine Hansen, Suaiba Salahuddin, Robert Jenssen, Marina Höhne, and Michael Kampffmeyer. Protovae: A trustworthy self-explainable prototypical variational model. In *Advances in Neural Information Processing Systems*, volume 35, pages 17940–17952. Curran Associates, Inc., 2022.
- [39] Mateusz Pach, Dawid Rymarczyk, Koryna Lewandowska, Jacek Tabor, and Bartosz Zieliński. Lucidppn: Unambiguous prototypical parts network for user-centric interpretable computer vision. *arXiv preprint arXiv:2405.14331*, 2024.
- [40] Robert van der Klis, Stephan Alaniz, Massimiliano Mancini, Cassio F. Dantas, Dino Ienco, Zeynep Akata, and Diego Marcos. Pdisconet: Semantically consistent part discovery for fine-grained recognition. In *Proc. IEEE/CVF International Conference on Computer Vision (ICCV)*, pages 1866–1876, 2023.
- [41] Zachariah Carmichael, Timothy Redgrave, Daniel Gonzalez Cedre, and Walter J Scheirer. This probably looks exactly like that: An invertible prototypical network. *arXiv preprint arXiv:2407.12200*, 2024.
- [42] Jon Donnelly, Alina Jade Barnett, and Chaofan Chen. Deformable protopnet: An interpretable image classifier using deformable prototypes. In *Proc. IEEE/CVF conference on computer vision and pattern recognition*, pages 10265–10275, 2022.
- [43] Stefano Frizzo Stefenon, Gurmail Singh, Kin-Choong Yow, and Alessandro Cimatti. Semi-protopnet deep neural network for the classification of defective power grid distribution structures. *Sensors*, 22(13):4859, 2022.
- [44] Sanaz Mohammadjafari, Mucahit Cevik, Mathusan Thanabalasingam, and Ayse Basar. Using protopnet for interpretable alzheimer’s disease classification. In *Canadian AI*, 2021.
- [45] Eunji Kim, Siwon Kim, Minji Seo, and Sungroh Yoon. Xprotonet: Diagnosis in chest radiography with global and local explanations. In *Proc. IEEE/CVF Conference on Computer Vision and Pattern Recognition (CVPR)*, pages 15719–15728, June 2021.
- [46] Gianluca Carloni, Andrea Berti, Chiara Iacconi, Maria Antonietta Pascali, and Sara Colantonio. On the applicability of prototypical part learning in medical images: Breast masses classification using protopnet. In *International Conference on Pattern Recognition*, pages 539–557. Springer, 2022.
- [47] Romain Xu-Darme, Georges Quénot, Zakaria Chihani, and Marie-Christine Rousset. Sanity checks for patch visualisation in prototype-based image classification. In

- Proc. IEEE/CVF Conference on Computer Vision and Pattern Recognition*, pages 3691–3696, 2023.
- [48] Adrian Hoffmann, Claudio Fanconi, Rahul Rade, and Jonas Kohler. This looks like that... does it? shortcomings of latent space prototype interpretability in deep networks. *arXiv preprint arXiv:2105.02968*, 2021.
- [49] Qihan Huang, Mengqi Xue, Wenqi Huang, Haofei Zhang, Jie Song, Yongcheng Jing, and Mingli Song. Evaluation and improvement of interpretability for self-explainable part-prototype networks. In *Proc. IEEE/CVF International Conference on Computer Vision*, pages 2011–2020, 2023.
- [50] Frank Willard, Luke Moffett, Emmanuel Mokel, Jon Donnelly, Stark Guo, Julia Yang, Giyoung Kim, Alina Jade Barnett, and Cynthia Rudin. This looks better than that: Better interpretable models with protopnext. *arxiv preprint arxiv:2406.14675*, 2024.
- [51] Romain Xu-Darme, Aymeric Varasse, Alban Grastien, Julien Girard, and Zakaria Chihani. Cabrnet, an open-source library for developing and evaluating case-based reasoning models. *arXiv preprint arXiv:2409.16693*, 2024.
- [52] Chiyu Ma, Brandon Zhao, Chaofan Chen, and Cynthia Rudin. This looks like those: Illuminating prototypical concepts using multiple visualizations. *Advances in Neural Information Processing Systems*, 36, 2024.
- [53] Meike Nauta, Annemarie Jutte, Jesper Provoost, and Christin Seifert. This looks like that, because... explaining prototypes for interpretable image recognition. In *Joint European Conference on Machine Learning and Knowledge Discovery in Databases*, pages 441–456. Springer, 2021.
- [54] Heng-Da Cheng, X. H. Jiang, Ying Sun, and Jingli Wang. Color image segmentation: advances and prospects. *Pattern recognition*, 34(12):2259–2281, 2001.
- [55] Wikipedia contributors. Hsl and hsv color spaces. [https://en.wikipedia.org/wiki/HSL\\_and\\_HSV](https://en.wikipedia.org/wiki/HSL_and_HSV), 2024. Accessed: 2024-10-28.
- [56] Thalles Silva and Adín Ramírez Rivera. Representation learning via consistent assignment of views to clusters. In *Proc. 37th ACM/SIGAPP Symposium on Applied Computing*, pages 987–994, 2022.
- [57] Mikołaj Sacha, Bartosz Jura, Dawid Rymarczyk, Łukasz Struski, Jacek Tabor, and Bartosz Zieliński. Interpretability benchmark for evaluating spatial misalignment of prototypical parts explanations. *arXiv preprint arXiv:2308.08162*, 2023.
- [58] Chong Wang, Yuyuan Liu, Yuanhong Chen, Fengbei Liu, Yu Tian, Davis J McCarthy, Helen Frazer, and Gustavo Carneiro. Learning support and trivial prototypes for interpretable image classification. *arXiv preprint arXiv:2301.04011*, 2023.
- [59] Romain Xu-Darme, Georges Quénot, Zakaria Chihani, and Marie-Christine Rousset. Sanity checks for patch visualisation in prototype-based image classification. In *Proc. IEEE/CVF Conference on Computer Vision and Pattern Recognition*, pages 3690–3695, 2023.
- [60] Srishti Gautam, Marina M-C Höhne, Stine Hansen, Robert Jenssen, and Michael Kampffmeyer. This looks more like that: Enhancing self-explaining models by prototypical relevance propagation. *Pattern Recognition*, 136:109172, 2023.
- [61] Sebastian Raschka. Model evaluation, model selection, and algorithm selection in machine learning. *arXiv preprint arXiv:1811.12808*, 2018.
- [62] Alexander Buslaev, Vladimir I. Iglovikov, Eugene Khvedchenya, Alex Parinov, Mikhail Druzhinin, and Alexandr A. Kalinin. Albu-mentations: Fast and flexible image augmentations. *Information*, 11(2), 2020. ISSN 2078-2489.
- [63] Meike Nauta, Jan Trienes, Shreyasi Pathak, Elisa Nguyen, Michelle Peters, Yasmin Schmitt, Jörg Schlötterer, Maurice van Keulen, and Christin Seifert. From anecdotal evidence to quantitative evaluation methods: A systematic review on evaluating explainable ai. *ACM Computing Surveys*, 55(13s): 1–42, 2023.